JACS
JOURNAL OF THE AMERICAN CHEMICAL SOCIETY
Article
pubs.acs.org/JACS

Intramolecular Iron-Mediated C−H Bond Heterolysis with an Assist of Pendant Base in a [FeFe]-Hydrogenase Model

Dehua Zheng,[†,#] Ning Wang,[‡,§,#] Mei Wang,*[,†] Shengda Ding,[‡] Chengbing Ma,[∥] Marcetta Y. Darensbourg,[‡] Michael B. Hall,*[,‡] and Licheng Sun[†,⊥]

[†]State Key Laboratory of Fine Chemicals, DUT-KTH Joint Education and Research Center on Molecular Devices, Dalian University of Technology (DUT), Dalian 116024, People's Republic of China

[‡]Department of Chemistry, Texas A&M University, College Station, Texas 77845, United States

[§]School of Chemistry and Chemical Engineering, Henan University of Technology, Zhengzhou 450001, People's Republic of China

[∥]State Key Laboratory of Structural Chemistry, Fujian Institute of Research on the Structure of Matter, Fuzhou 350002, People's Republic of China

[⊥]Department of Chemistry, KTH Royal Institute of Technology, Stockholm 10044, Sweden

Supporting Information

ABSTRACT: Although many metalloenzymes containing iron play a prominent role in biological C−H activation processes, to date iron-mediated C(sp^3)−H heterolysis has not been reported for synthetic models of Fe/S-metalloenzymes. In contrast, ample precedent has established that nature's design for reversible hydrogen activation by the diiron hydrogenase ([FeFe]-H_2ase) active site involves multiple irons, sulfur bridges, a redox switch, and a pendant amine base, in an intricate arrangement to perform H−H heterolytic cleavage. In response to whether this strategy might be extended to C−H activation, we report that a [FeFe]-H_2ase model demonstrates iron-mediated intramolecular C−H heterolytic cleavage via an agostic C−H interaction, with proton removal by a nearby pendant amine, affording Fe^{II}−[Fe'^{II}−CH−S] three-membered-ring products, which can be reduced back to **1** by Cp_2Co in the presence of HBF_4. The function of the pendant base as a proton shuttle was confirmed by the crystal structures of the N-protonated intermediate and the final deprotonated product in comparison with that of a similar but pendant-amine-free complex that does not show evidence of C−H activation. The mechanism of the process was backed up by DFT calculations.

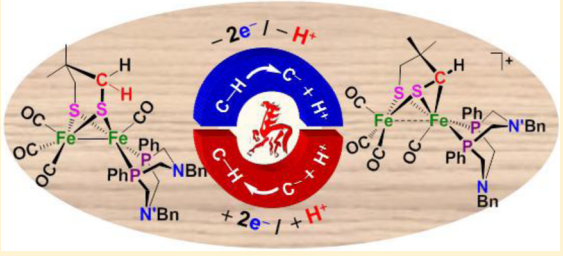

INTRODUCTION

The remarkable efficiency of [FeFe]-hydrogenase ([FeFe]-H_2ase) enzymes is related to an equally remarkable arrangement of components that provide a low-energy pathway for H−H bond cleavage and formation. Many lines of evidence point to the function of an amine base, strategically placed in a dithiolate cofactor, as a shuttle for protons transferring to and from the Fe_d (the iron distal to the 4Fe4S cluster that acts as a redox level switch to the two iron subsite), to assist the proton-coupled electron transfer processes.[1−9] Inspired by the important structural pendant base feature of [FeFe]-H_2ases, DuBois and co-workers devised a series of pendant amine base containing diphosphine ligands that optimize mononickel and monoiron complexes as sustainable, highly active base-metal catalysts for H−H heterolytic formation and cleavage.[10−15] Additional studies made by us and others have determined that the internal amine in such chelating diphosphine ligands installed on [FeFe]-H_2ase active site models can also act as a proton transfer relay and facilitate iron-catalyzed reduction of protons and oxidation of hydrogen.[16−22]

In the process of catalytic activation of H_2 with transition metals, the σ-type (η^2-H_2)·M interaction can lead to both homolytic and heterolytic H−H cleavage, with the former being prominent with readily oxidizable (typically third row) transition metals; the latter occurs with electrophilic metals in the presence of external bases. Despite similar homolytic H−H and C−H bond energies, the steric encumbrance from carbon substituents, as well as the directionality of orbital overlap, has relegated activation of C(sp^3)−H bonds largely to noble metals under harsh conditions.[23] As functional group tolerance is a requirement of most synthetic applications in organic chemistry, research into C−H activation under mild and sustainable conditions is a worthy and ongoing challenge to chemists.[24]

Herein we report an intramolecular iron-mediated C(sp^3)−H heterolysis in double oxidation of an [FeFe]-H_2ase model under ambient conditions, with an assist of the pendant amine base of a diphosphine ligand. Figure 1 shows the parent

Received: July 31, 2014
Published: September 22, 2014

   dx.doi.org/10.1021/ja5078014 | J. Am. Chem. Soc. 2014, 136, 16817−16823

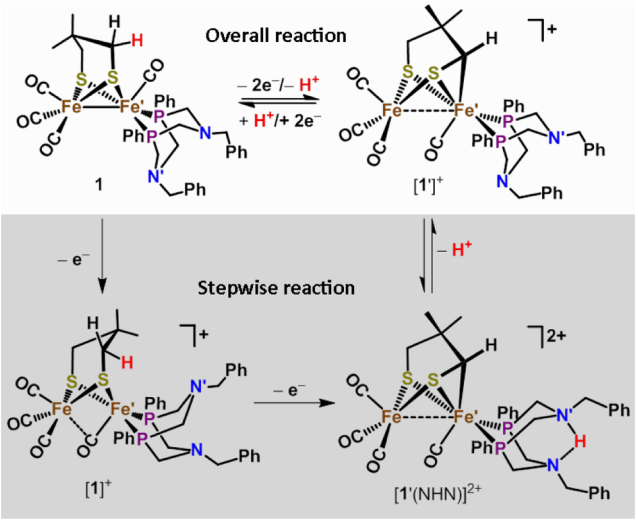

Figure 1. Summary of the oxidation reaction of **1**. The top half summarizes the overall reaction discovered in this work, and the bottom shaded area gives the observed intermediates.

complex of this study, (μ-dmpdt)[Fe(CO)$_3$][Fe′(CO)($P^{Ph}_2N^{Bn}_2$)] (**1**; dmpdt = 2,2-dimethyl-1,3-propanedithiolate; $P^{Ph}_2N^{Bn}_2$ = 1,5-dibenzyl-3,7-diphenyl-1,5-diaza-3,7-diphosphacyclooctane), along with products derived from oxidation and deprotonation. The structures of **1**, [**1**′(NHN)]$^{2+}$, and [**1**′]$^+$ presented in Figure 1 reflect the configurations obtained from X-ray diffraction analyses (Figure 2); the structure indicated for [**1**]$^+$ was assigned according to IR and EPR spectral data along with computational studies. The reaction process is an account of competition between two Lewis bases, the C–H σ-bond and the lone pair electrons of the pendant amine, for the Lewis acid site of iron. The ultimate path to stability requires a synchrony of molecular motions that creates a favorable structure with a six-coordinate Fe^{II}, an Fe–C bond, and a protonated amine. DFT studies have identified a mechanistic pathway for the experimentally observed C–H activation with illustration of the roles played by the versatile pendant amine.

RESULTS AND DISCUSSION

Synthesis and Characterization of 1 and 2. Complex **1** was prepared in moderate yield from the reaction of (μ-dmpdt)[Fe(CO)$_3$]$_2$ with $P^{Ph}_2N^{Bn}_2$ in refluxing THF in the presence of Me$_3$NO·2H$_2$O.[25] A similar reaction using $P^{Ph}_2C_5$ as ligand (as a pendant-base-free reference for studies of **1**) afforded only one configurational isomer, **2**, in which the six-membered ring in a chair conformation is adjacent to the apical CO and the five-membered ring is close to the basal COs of the other iron center[14] but is otherwise a structural analogue to **1**. Complexes **1** and **2** were well characterized by IR, ^{1}H and ^{31}P{^{1}H} NMR spectroscopy, and mass spectrometry. The structures of **1** and **2**, determined by X-ray diffraction analyses (Figure 2a,b), are very similar; both contain a 2Fe2S core in a butterfly conformation, a diphosphine ligand coordinating to an iron (which we will hereafter refer to as Fe′) in basal–basal positions, and the top Fe′PCXCP ring (**1**, X = N; **2**, X = C) featuring a chair conformation in the solid state.

Oxidation of 1 and 2. The chemical oxidation of **1** in CH$_2$Cl$_2$ was monitored by in situ IR spectroscopy at 20 °C under argon. Upon addition of 1 equiv of FcBF$_4$ or FcBAr$^F_4$, the CO absorptions of **1** (ν_{CO} 2018, 1943, and 1894 cm^{-1}; Figure 3a) rapidly disappeared, accompanied by the appearance of two new bands at higher energy (ν_{CO} 2086 and 2028 cm^{-1};

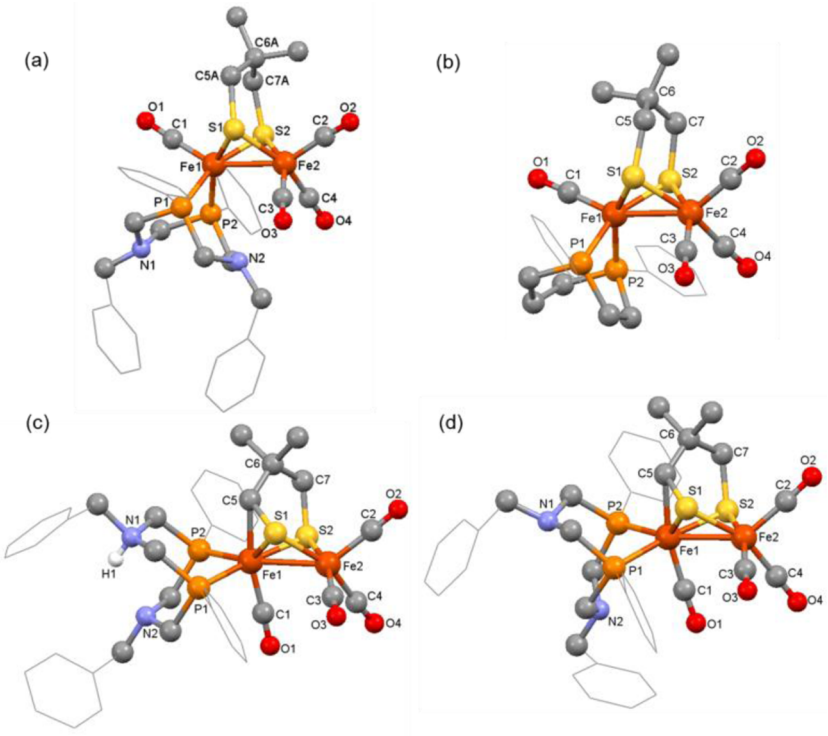

Figure 2. Molecular structures of (a) **1**, (b) **2**, and the cations in (c) [**1**′(NHN)](BF$_4$)$_2$ and (d) [**1**′]BAr$^F_4$ as ball and stick drawings. Hydrogen atoms are omitted except for the H attached to N1 in [**1**′(NHN)](BF$_4$)$_2$. Full details of metric data are provided in Tables S1–S4 (Supporting Information).

dx.doi.org/10.1021/ja5078014 | J. Am. Chem. Soc. 2014, 136, 16817–16823

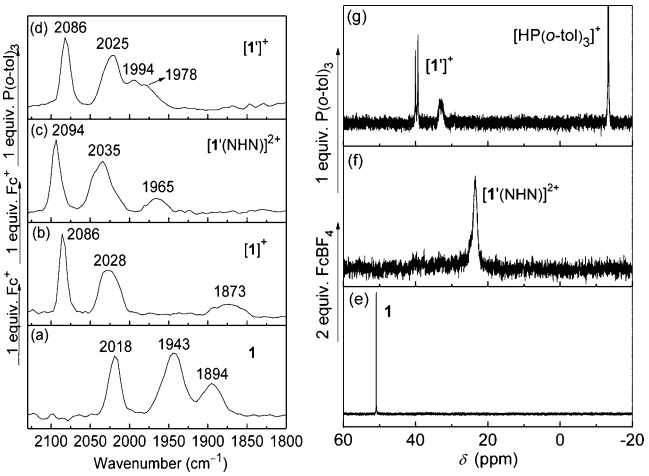

Figure 3. ν_{CO} IR spectral monitoring of the in situ formed oxidation products of **1** in CH_2Cl_2: (a) **1**; (b) $[\mathbf{1}]^+$; (c) $[\mathbf{1}'(NHN)]^{2+}$; (d) deprotonation with P(*o*-tol)$_3$ to yield $[\mathbf{1}']^+$. $^{31}P\{^1H\}$ NMR spectral monitoring of the in situ produced diamagnetic compounds in CD_2Cl_2: (e) **1**; (f) $[\mathbf{1}'(NHN)]^{2+}$; (g) $[\mathbf{1}']^+$.

Figure 3b and Figure S1a (Supporting Information)), and a third weak and broad band appeared at ca. 1873 cm^{-1}, indicative of a bridging or semibridging CO. In analogy to previously reported $Fe^{II}Fe^{I}$ models of the H_{ox} redox of [FeFe]-H_2ase, these changes in the ν_{CO} region are indicative of formation of the mixed-valence species $[\mathbf{1}]^+$ at an $Fe^{II}Fe'^{I}$ redox level containing a semibridging CO ligand.[25−29]

The X-band EPR spectrum of $[\mathbf{1}]BAr^F_4$ measured in liquid CH_2Cl_2/toluene at 20−22 °C is a triplet, with a *g* value of 2.059 and the coupling constant A(P) = 67.79 MHz (Figure S2b (Supporting Information)). At −163 °C in frozen CH_2Cl_2/toluene solution, a rhombic EPR spectrum (Figure 4a) is obtained, from which are derived principal $g_{x,y,z}$ values at 2.126, 2.022, and 2.017 with triplet overlays of $A_{x,y,z}$(P) = 72.90, 61.97, and 70.13 MHz, respectively. Both spectra are consistent with ^{31}P superhyperfine coupling (SHFC) of the unpaired electron with two equivalent phosphorus nuclei within the coordination sphere of a d^7 Fe'^{I}. A similar explanation was offered for the liquid and frozen solution EPR spectra of the mixed-valence cations $[(\mu\text{-}SCH_2CH_2CH_2S)(\mu\text{-}CO)\{Fe(dppv)\}\{Fe(CO)_2PMe_3\}]^+$ and $(\mu\text{-}SCH_2C(CH_3)_2CH_2S)(\mu\text{-}CO)\{Fe(CO)(PMe_3)\}\{Fe(CO)_2PMe_3\}]^+$, which have ^{31}P SHFC values of ca. 75 MHz.[28,29]

Addition of another 1 equiv of Fc^+ to the solution of $[\mathbf{1}]^+$ resulted in blue shifts of all the ν_{CO} absorptions (Figure 3c). Upon addition of 1 equiv of P(*o*-tol)$_3$ as a noncoordinating Brønsted base, the three new bands at 1965, 2035, and 2094 cm^{-1}, ultimately attributed to $[\mathbf{1}'(NHN)]^{2+}$, instantly shifted to 2086, 2025, 1994, and 1978 cm^{-1} (Figure 3d), representing the final deprotonated product $[\mathbf{1}']^+$ (Figure S3 (Supporting Information)). This is the reaction sequence summarized in Figure 1.

In CH_2Cl_2 at 20 °C, $[\mathbf{1}'(NHN)]^{2+}$ gradually converts to $[\mathbf{1}']^+$ even in the absence of deliberately added base (Figure S1b (Supporting Information)); the instability is presumably due to a trace of water. However, the $[\mathbf{1}']BAr^F_4$ salt is stable in CH_2Cl_2 over several hours at room temperature, as indicated by further IR spectral monitoring. Of particular interest, both $[\mathbf{1}']^+$ and $[\mathbf{1}'(NHN)]^{2+}$ can be rapidly reduced back to **1** by Cp_2Co in the presence of HBF_4 (Figure S4 (Supporting Information)), indicative of the re-formation of the C−H bond.

The one-electron oxidation of **2**, a reference complex sans pendant base, by 1 equiv of $FcBF_4$ in CH_2Cl_2 at −78 °C was also monitored by in situ IR spectroscopy, indicating the formation of two products (Figure S5 (Supporting Information)). Together with bands of greater intensity in the terminal CO region, two weak bands at 1890 and 1853 cm^{-1} are indicative of the existence of a semibridging CO ligand in both of the oxidized products. We assume that two isomers of $[\mathbf{2}]^+$, both of which feature a (semi)bridging carbonyl, arise from rotations of either of the FeL_3 moieties.[30,31] Computational studies yield ν_{CO} frequencies that match the experimental values (Figure S6 (Supporting Information)). The most important difference in the oxidation reactivities of **1** and **2** is that **2**, with no pendant base, could not be doubly oxidized even in the presence of a large excess of $FcBF_4$.

Further Characterization and the Structures of Doubly Oxidized Products $[\mathbf{1}'(NHN)]^{2+}$ and $[\mathbf{1}']^+$. From addition of 2 equiv of $FcBF_4$ in CH_2Cl_2 the doubly oxidized product $[\mathbf{1}'(NHN)](BF_4)_2$ was obtained as a violet solid by crystallization from CH_2Cl_2/hexane at 0 °C. The purple-red complex $[\mathbf{1}']^+$ was isolated from the deprotonation of freshly

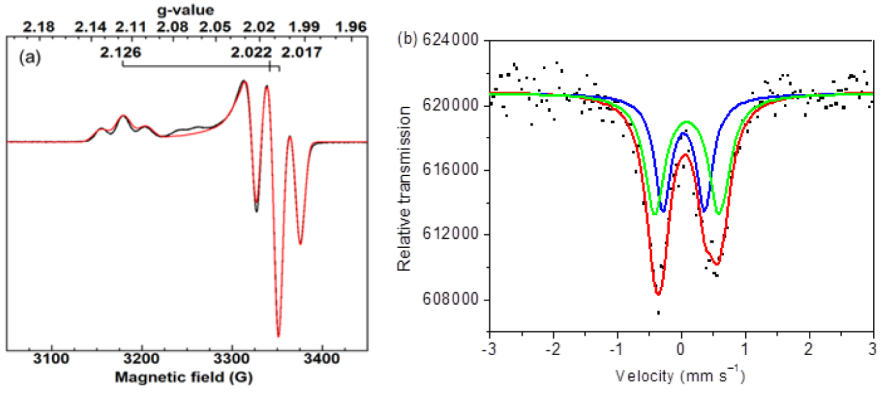

Figure 4. (a) EPR experimental (black) and simulated spectra (red) of paramagnetic $[\mathbf{1}]^+$ in frozen CH_2Cl_2/toluene (1/1 v/v) at −163 °C. The simulation (Lorentzian line shape) gives $g_{x,y,z}$ = 2.126, 2.022, and 2.017 and hyperfine constants for two phosphorus atoms $A_{x,y,z}$(P) = 72.90, 61.97, and 70.13 MHz. (b) Mössbauer spectrum of $[\mathbf{1}'](BF_4)$ at 80 K. The green and blue lines are the results of least-squares fits with the nested-doublet configuration, giving isomer shifts of $\delta_{1,2}$ = −0.04 and −0.09 mm s^{-1} and quadrupole splittings of $\Delta E_{Q1,2}$ = 0.66 and 1.02 mm s^{-1} with line widths of 0.30 and 0.38 mm s^{-1}.

dx.doi.org/10.1021/ja5078014 | J. Am. Chem. Soc. 2014, 136, 16817−16823

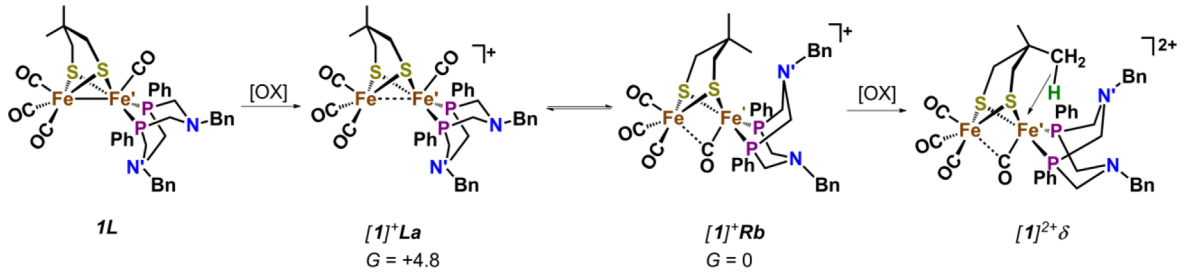

Figure 5. Key species in the two successive oxidation steps of **1**. Energy values are given in kcal mol^{-1}.

generated $[\mathbf{1}'(\mathrm{NHN})]^{2+}$. Isolated salts of $[\mathbf{1}']^{+}$ and $[\mathbf{1}'(\mathrm{NHN})]^{2+}$ show parent ions in the high-resolution mass spectrometric analysis. Consistent with the in situ IR spectral results, a sharp singlet at δ 50.90 in the $^{31}P\{^{1}H\}$ NMR spectrum of **1** (Figure 3e) shifts to δ 23.54 in that of $[\mathbf{1}'(\mathrm{NHN})]^{2+}$ (Figure 3f). Concurrently, a low-field signal appeared at δ 11.16 in the ^{1}H NMR spectrum, which is consistent with the signature chemical shift (δ 11.7) reported for the proton bridging between two amine-N atoms (N−H···N) in the protonated $P^{Ph}{}_2N^{Bn}{}_2$ ligand of DuBois' nickel complexes.[32] The broad signal at δ 23.54 is resolved into two doublets in the $^{31}P\{^{1}H\}$ NMR spectrum of isolated $[\mathbf{1}'(\mathrm{NHN})]^{2+}$ measured at low temperature. The variable-temperature (+20 to −30 °C) $^{31}P\{^{1}H\}$ NMR spectra (Figure S7 (Supporting Information)) of $[\mathbf{1}'(\mathrm{NHN})]^{2+}$ indicate a fluxional process associated with the $P^{Ph}{}_2N^{Bn}{}_2$ ligand in solution at room temperature, similar to the fast equilibrium of the multiple conformations of $Fe'P_2C_2N$ metallocyclohexanes observed for a mononuclear iron complex containing a P_2N_2 ligand in solution.[33]

Upon addition of 1 equiv of P(*o*-tol)$_3$ to the CD_2Cl_2 solution of $[\mathbf{1}'(\mathrm{NHN})]^{2+}$, the broad $^{31}P\{^{1}H\}$ NMR signal at δ 23.54 completely disappears, accompanied by the appearance of two doublets for $[\mathbf{1}']^{+}$ at δ 30.87 (d, J_{pp} = 106.8 Hz) and 38.90 (d, J_{pp} = 103.6 Hz) (Figure 3g), indicating different chemical environments for the phosphorus donors. Simultaneously, a typical ^{31}P resonance for $[HP(o\text{-tol})_3]^{+}$ is observed at δ −13.59. As predicted, the signal at δ 11.16 in the ^{1}H NMR spectrum also disappeared with addition of P(*o*-tol)$_3$. In addition to the expected ^{1}H NMR signals for CH_2 and CH_3 groups in the region of δ 1.2−3.9 and for the phenyl group at δ 7.1−7.7, a signal appears at δ 4.17 for $[\mathbf{1}']^{+}$. This resonance, which was also detected in the ^{1}H NMR spectrum of $[\mathbf{1}'(\mathrm{NHN})]^{2+}$, is attributed to the hydrogen of methine in the Fe′SC three-membered ring that was positively established in both $[\mathbf{1}'(\mathrm{NHN})]^{2+}$ and $[\mathbf{1}']^{+}$ by crystallography.

The molecular structures presented in Figure 2c,d indicate that the framework of $[\mathbf{1}'(\mathrm{NHN})]^{2+}$ has only trivial differences from that of $[\mathbf{1}']^{+}$. The Fe···Fe′ distances are the same for $[\mathbf{1}'(\mathrm{NHN})]^{2+}$ and $[\mathbf{1}']^{+}$, about 2.626 Å, which is longer than that of **1** (2.562 Å). Clearly the major difference in the three structures is the presence of a Fe′−C bond in $[\mathbf{1}'(\mathrm{NHN})]^{2+}$ and $[\mathbf{1}']^{+}$, within a Fe′−S−C three-membered ring. This is, to our knowledge, unprecedented in the hundreds of $(\mu\text{-}SCH_2XCH_2S)[Fe(CO)_3]_2$ species and derivatives that have thus far been reported. Such an alteration of the bridging dithiolate cofactor generates a six-coordinate, pseudo-octahedral iron in which the phosphorus donors are retained trans to the bridging thiolates and the carbonyl ligand is trans to the methine carbon, with $\angle C5\text{−}Fe'\text{−}C1_{CO}$ = 166°. The CO placed under the Fe−Fe′ vector with ∠Fe′−C1−O1 = 176° does not have the characteristics of a bridging CO. Despite such an unusual modification of the coordination geometry at the P-substituted iron, the $Fe(CO)_3$ unit and its relation to the substantially altered bridging dithiolate are largely unchanged.

A noticeable contrast in the structures of $[\mathbf{1}'(\mathrm{NHN})]^{2+}$ and $[\mathbf{1}']^{+}$ is that, in the latter, the top $Fe'P_2C_2N$ metallacyclohexane is in a chair conformation while the bottom ring adopts the boat form. In $[\mathbf{1}'(\mathrm{NHN})]^{2+}$, both $Fe'P_2C_2N$ rings are in chair conformations, giving a site for a proton to reside between the two amine-N atoms. Indeed, as has been found in DuBois' other "pinched", or exo, ligand conformations,[12] such a hydrogen atom (H1) was indicated from Fourier difference maps, with N1−H1 0.902 Å and N2···H1 2.199 Å. The N1···N2 distance (2.806(8) Å) in $[\mathbf{1}'(\mathrm{NHN})]^{2+}$ is ca. 0.8 Å shorter than that in $[\mathbf{1}']^{+}$. Taken together, the spectroscopic and crystallographic data indicate that the two-electron-oxidation reaction of **1** to $[\mathbf{1}']^{2+}$ proceeds via an intramolecular proton transfer from one of the SCH_2 units to the internal amine bases of the $P^{Ph}{}_2N^{Bn}{}_2$ ligand, giving the novel diiron complex $[\mathbf{1}'(\mathrm{NHN})]^{2+}$, which readily loses a proton to form $[\mathbf{1}']^{+}$.

The Mössbauer spectrum of $[\mathbf{1}'](BF_4)$ measured at 80 K consists of two broad lines that can be best simulated by two quadrupole-split doublets of roughly equal intensities (Figure 4b), with the isomer shifts $\delta_{1,2}$ = −0.04 and −0.09 mm s^{-1} and the quadrupole splittings $\Delta E_{Q1,2}$ = 0.66 and 1.02 mm s^{-1}. The small δ values are consistent with low-spin Fe^{II} sites, as reported for other Fe^{II}-containing hydrogenase mimics.[34,35] The significant difference in the quadrupole-splitting parameters reflects complex $[\mathbf{1}']^{+}$ featuring two Fe^{II} centers in disparate coordination environments,[36,37] which is consistent with its X-ray crystal structure (Figure 2d).

Address of Mechanism for Activation of the C−H Bond in 1 on the Basis of Computational Studies. Hereafter the designations of all computed species are given in italics to distinguish them from their experimental counterparts. The atoms that are directly involved in the β-C−H bond activation are marked with a prime: C′, H′, N′, and Fe′.

The computational study reveals that ***1L*** (Figure 5), with the bridgehead of the FeS_2C_3 ring pointing toward the $Fe(CO)_3$ moiety, is 4.6 kcal mol^{-1} more stable than its counterpart ***1R***, featuring the bridgehead oriented toward the $Fe'(CO)(P_2N_2)$ unit. One-electron oxidation of ***1L*** directly produces ***[1]+La*** with a geometry like that of ***1L***. Overcoming a few barriers no higher than 6.1 kcal mol^{-1}, ***[1]+La*** converts into ***[1]+Rb***, the most stable isomer of $[\mathbf{1}]^{+}$ (Figure S8 (Supporting Information) for the conformers of $[\mathbf{1}]^{+}$, created by rotations and bridgehead orientation). ***[1]+Rb*** features a bridgehead methyl pointing toward the vacant site of rotated $Fe'(CO)(P_2N_2)$ moiety with the apical CO beneath the S_2P_2 plane. The rotation of $Fe'(CO)(P_2N_2)$ and (semi)bridging carbonyl reduces the Fe−Fe′ bond character on the SOMO. Concomitantly, the spin density resides on Fe′ (Figure S9

dx.doi.org/10.1021/ja5078014 | J. Am. Chem. Soc. 2014, 136, 16817−16823

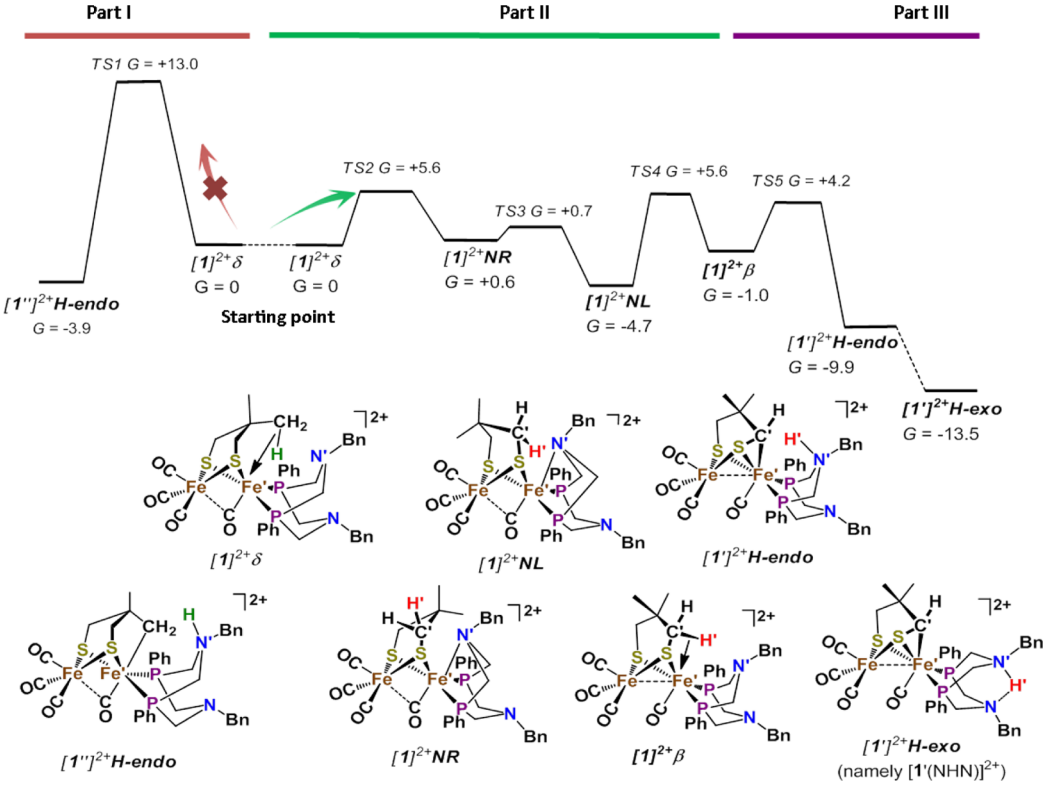

Figure 6. Energy profile of β-C−H bond activation and related intermediates. The energy profile (in kcal mol^{-1}) contains three parts: (I) direct activation of the δ-C−H bond (the direction of the reaction in part I is from "starting point" to the left); (II) conversion between the δ-agostic interaction and β-agostic interaction; (III) activation of the β-C−H bond aided by the pendant amine base.

(Supporting Information)), consistent with the observed ^{31}P hyperfine couplings in the EPR spectrum of $[\mathbf{1}]^+$ (Figure 4a). An oxidation state assignment of $Fe^{II}Fe'^{I}$ is given to $[\mathbf{1}]^+\boldsymbol{Rb}$, similar to the case for the precedented H_{ox} models.[25−29,38] A weak interaction between a hydrogen from the bridgehead methyl and the iron vacant site (d(Fe′−H) = 2.579 Å, d(C−H) = 1.103 Å) is realized and may contribute to the overall stabilization of $[\mathbf{1}]^+\boldsymbol{Rb}$.[39]

Further oxidation of $[\mathbf{1}]^+\boldsymbol{Rb}$ yields $[\mathbf{1}]^{2+}\boldsymbol{\delta}$, with concomitant formation of a two-electron δ-agostic interaction[40−42] between the δ-C−H bond on the bridgehead methyl and Fe′ (d(Fe′−H) = 1.844 Å, d(C−H) = 1.145 Å). Such a δ-agostic interaction in $[\mathbf{1}]^{2+}\boldsymbol{\delta}$ could not lead to the δ-C−H activation, due to a relatively high barrier (13.0 kcal/mol) of ***TS1*** (part I in Figure 6). The high barrier is likely attributed to a combination of poor positioning of the C−H bond relative to Fe′ (poor overlap of orbitals), the introduction of steric strain into the originally relaxed $Fe'S_2C_3$ ring, and the lower availability of pendant amine (d(N′···H) = 2.388 Å in $[\mathbf{1}]^{2+}\boldsymbol{\delta}$, in comparison to d(N′···H′) = 2.234 Å in $[\mathbf{1}]^{2+}\boldsymbol{\beta}$ discussed later; Figure S10 (Supporting Information)). In fact, there is an alternative pathway leading to the experimentally observed product $[\mathbf{1}'(NHN)]^{2+}$ with a series of lower barriers.

This lower energy path (Figure 6, parts II and III) begins with the displacement of the δ-agostic interaction by a strained Fe′−N′ interaction from the pendant amine, overcoming a shallow barrier ***TS2*** of 5.6 kcal mol^{-1} to form $[\mathbf{1}]^{2+}\boldsymbol{NR}$. The dative bond between Fe′ and N′ (d(Fe′−N′) = 2.234 Å) is not optimal due to the steric strain of the Fe′PCNCP ring; it is elongated in comparison to a bond between Fe^{II} and an analogous free amine (shorter by ∼0.15 Å, Figure S11 (Supporting Information)). Nevertheless, the pendant amine serves as a "placeholder" in $[\mathbf{1}]^{2+}\boldsymbol{NR}$, to occupy the vacant site and saturate the coordination potential of Fe'^{II}. The entire structure further stabilizes itself by swinging the $Fe'S_2C_3$ ring from the boat conformation in $[\mathbf{1}]^{2+}\boldsymbol{NR}$ to the chair in $[\mathbf{1}]^{2+}\boldsymbol{NL}$ through ***TS3***. A consequence of such boat−chair conversion is that the β-C′−H′ bond on the dithiolate linker is brought close to Fe′ in $[\mathbf{1}]^{2+}\boldsymbol{NL}$. At this stage, the "placeholder" pendant amine could be replaced by a β-agostic interaction, as shown in $[\mathbf{1}]^{2+}\boldsymbol{\beta}$. During this replacement the $Fe'S_2C_3$ ring distorts, as reflected in ***TS4*** (see the movie in the Supporting Information). The distortion helps the β-C′−H′ bond approach Fe′ sufficiently closely that a σ complex could be formed, in which the β-C′−H′ bond length (d(C′−H′) = 1.184 Å) is significantly elongated; the distortion also reorganizes the coordination environment, especially reducing the Fe′···H′, Fe′···C′, and N′···H′ distances (d(Fe′···H′) = 1.802 Å, d(Fe′···C′) = 2.308 Å, d(N′···H′) = 2.308 Å), in a way that leads to facile β-C′−H′ bond heterolysis. Eventually, the β-C′−H′ activation occurs in a concerted fashion; as the proton cleaved from the β-C′−H′ bond transfers to the pendant amine, the residual electron pair on carbon forms the Fe′−C′ bond, producing $[\mathbf{1}']^{2+}\boldsymbol{H\text{-}endo}$. The proton at the internal amine could transfer from the endo to the exo position, forming the more stable species $[\mathbf{1}']^{2+}\boldsymbol{H\text{-}exo}$, in which the proton is pinched and stabilized by two pendant amines of the P_2N_2 ligan,d as shown in the crystal structure of $[\mathbf{1}'(NHN)]^{2+}$. Similar proton transfer has been reported by DuBois et al. for the mononuclear nickel complexes containing a P_2N_2 ligand.[43,44] The experimental results clearly show that the proton at the internal amine can be permanently removed by an extrinsic base to form the final product $[\mathbf{1}']^+$.

dx.doi.org/10.1021/ja5078014 | J. Am. Chem. Soc. 2014, 136, 16817−16823

CONCLUSIONS

Two-electron oxidation of the [FeFe]-H_2ase model (**1**) bearing a $P^{Ph}{}_2N^{Bn}{}_2$ ligand with pendant amine bases leads to an intramolecular iron-mediated C−H heterolysis. In fact, such a C−H bond activation cannot take place for the analogue, complex **2**, having a $P^{Ph}{}_2C_5$ without the built-in, pendant base. The contrasting oxidative reactivities of **1** and **2** clearly indicate that the pendant amine in the second coordination sphere plays a critical role in the C−H heterolysis. The pendant amine serves as a final proton shuttle and also as a regulator of molecular transformation during the process of C−H heterolysis. The doubly oxidized product $[\mathbf{1}']^+$ is an unique diiron complex with a rigid FeSC three-membered ring while having no (semi)bridging CO. It is of interest that the process is reversed by reduction of $[\mathbf{1}']^+$ in the presence of Brønsted acid. From the computations, an unexpectedly low barrier vibrational movement, involving distortion of the six-membered FeS_2C_3 ring containing the dithiolate cofactor along a particularly soft C−S−Fe compression, reorganizes the molecule to such an extent that a Fe···η^2-CH β-agostic interaction is established. This displacement, which surprisingly has a barrier comparable to that of the conventional chair−boat conversion, paves the way for further C−H bond activation. The deprotonation of η^2-CH takes place with the help of the pendant amine base. These findings endow the already capable dithiolate cofactor in [FeFe]-H_2ase mimics with further versatility in reactions. The C−H heterolysis under ambient conditions reveals that the [FeFe]-H_2ase mimics feature the capacity of stabilizing reactive anions: i.e., the carbanion in the present case or the hydride when H_2 is a substrate. These results shed light on the advantage of incorporation of a pendant amine base into a chelating diphosphine ligand, the platform for mononuclear nickel complexes in H−H heterolytic cleavage.[10,11] Such a strategy may be extended to C(sp^3)−H bond activation by iron using properly designed Lewis acid−base complexes.

EXPERIMENTAL SECTION

Materials and Methods. The compounds [(μ-dmpdt)$Fe_2(CO)_6$], 1,5-dibenzyl-3,7-diphenyl- 1,5-diaza-3,7-diphosphacyclooctane ($P^{Ph}{}_2N^{Bn}{}_2$), 1,4-diphenyl-1,4-diphosphacycloheptane ($P^{Ph}{}_2C_5$), and $FcBAr^F{}_4$ were prepared according to the literature procedures.

Infrared spectra were recorded on a JASCO FT/IR 430 spectrometer. ^{1}H and ^{31}P{^{1}H} NMR spectra were collected with a Varian INOVA 400 NMR instrument. In situ IR spectra were recorded on a Mettler-Toledo React-IR 15 System equipped with an MCT detector and a Dsub AgX SiComp in situ probe. Mass spectra were measured on a Q-TOF-Micro instrument (Waters). Elemental analyses were performed with a Thermoquest-Flash EA 1112 elemental analyzer. The single-crystal X-ray diffraction data were collected with a Bruker Smart Apex II CCD diffractometer with graphite-monochromated Mo Kα radiation (λ = 0.071073 Å) at 296(2) K using the ω−2θ scan mode. EPR spectra were collected with a Bruker A200-9.5/12 electron-spin resonance spectrometer equipped using an A-series X-band high-sensitivity optical resonator. The ^{57}Fe Mössbauer spectrum was recorded at 80 K on a Topologic 500A spectrometer. Additional experimental details can be found in the Supporting Information.

(μ-dmpdt)[Fe(CO)$_3$][Fe(CO)($P^{Ph}{}_2N^{Bn}{}_2$)] (1). The ligand PhP-{$CH_2NCH_2(CH_2Ph)$}$_2$PPh (0.48 g, 1.0 mmol) was added to the THF solution (40 mL) of (μ-dmpdt)$Fe_2(CO)_6$ (0.41 g, 1.0 mmol) in the presence of 2 equiv (0.22 g, 2.0 mmol) of $Me_3NO{\cdot}2H_2O$. The red solution was refluxed for 2 h, and then the solvent was removed under reduced pressure. The residue was purified by chromatography on a silica gel column with hexane/CH_2Cl_2 (3/1 v/v) as eluent. Complex **1** was obtained as a red powder from the collected yellow band after removal of solvent. Yield: 48% (0.40 g). ^{1}H NMR ($CDCl_3$): δ 7.51, 7.39, 7.31, 7.07, and 6.69 (20H, $4C_6H_5$), 4.06 and 3.65 (2s, 4H, $2NCH_2Ph$), 3.20, 3.12, 2.9, and 2.72 (4d, 8H, J = 12 Hz, $4PCH_2N$), 1.99 (d, 2H, J = 16 Hz, SCH_2C), 1.67 (d, 2H, J = 12 Hz, SCH_2C), 1.05 (s, 3H, CCH_3), 0.71 (s, 3H, CCH_3). ^{31}P{^{1}H} NMR ($CDCl_3$): δ 50.9 (s). IR (CH_2Cl_2): ν_{CO} 2018, 1943, 1894 cm^{-1}. Anal. Calcd (found) for $C_{39}H_{42}Fe_2N_2O_4P_2S_2$: C, 55.73 (55.60); H, 5.04 (4.97); N, 3.33 (3.29).

(μ-dmpdt)[Fe(CO)$_3$][Fe(CO)($P^{Ph}{}_2C_5$)] (2). Complex **2** was prepared as a red powder by a procedure essentially identical with the preparation of complex **1** but using $P^{Ph}{}_2C_5$ (0.29 g, 1.0 mmol) as ligand in toluene. Yield: 38% (0.25 g). ^{1}H NMR ($CDCl_3$): δ 7.58−7.36 (m, 10H, 2Ph), 2.89 (m, 2H, $P(CH_2)_3P$), 2.65 (m, 1H, $P(CH_2)_3P$), 2.04 (m, 1H, $P(CH_2)_3P$), 1.95 (m, 2H, $P(CH_2)_2P$), 1.92 (m, 2H, $P(CH_2)_2P$), 1.80 (m, 2H, $P(CH_2)_3P$), 1.78 (br s, 4H, SCH_2C), 0.96 (br s, 3H, CCH_3), 0.92 (s, 3H, CCH_3). ^{31}P{^{1}H} NMR ($CDCl_3$): δ 53.27. IR (CH_2Cl_2): ν_{CO} 2015, 1941, 1895 cm^{-1}. Anal. Calcd (found) for $C_{26}H_{30}Fe_2O_4P_2S_2$: C, 48.51 (48.47); H, 4.68 (4.69).

[1′]BAr$^F{}_4$. The oxidant $FcBAr^F{}_4$ (0.53 g, 0.5 mmol) was added to the CH_2Cl_2 solution (25 mL) of **1** (0.21 g, 0.25 mmol). The solution was stirred for 5 h at 25 °C, and then hexane was added (400 mL) to precipitate the product. A purple-red powder was deposited from the solvent and washed several times with hexane. Yield: ∼80% (0.34 g). ^{1}H NMR (CD_2Cl_2): δ 7.68−7.17 (m, 32H, $4C_6H_5$ and $4C_6H_3$-3,5-$(CF_3)_2$), 4.17 (br s, 1H, FeC(H)S), 3.90 (br s, 4H, $2NCH_2Ph$), 3.56−2.86 (m, 8H, $4PCH_2N$), 2.74 and 1.97 (2d, 2H, J = 12 Hz, SCH_2C), 1.23 (s, 6H, $2CH_3$). ^{31}P{^{1}H} NMR (CD_2Cl_2): δ 30.87 (d, J_{PP} = 106.8 Hz) and 38.90 (d, J_{PP} = 103.6 Hz). IR (CH_2Cl_2): ν_{CO} 2086, 2025, 1999, and 1978 cm^{-1}. ESI-HRMS: m/z 839.0678 (calcd for $[M]^+$, 839.0682).

[1′(NHN)](BF$_4$)$_2$. The oxidant $FcBF_4$ (0.027 g, 0.1 mmol) was added to a CH_2Cl_2 solution (5 mL) of **1** (0.042 g, 0.05 mmol) at 0 °C. The solution was stirred for 5 min, and then cooled hexane (25 mL) was added to form precipitates and the supernatant was filtered. The violet crude product was washed with pentane (2 × 2.5 mL) to further remove impurities. Yield: 92.0% (0.05 g). ^{1}H NMR (CD_2Cl_2) at −30 °C: δ 11.16 (br, 1H, N−H···N), 7.90−7.10 (m, 20H, $4C_6H_5$), 4.59 (br s, 2H, N(H)CH_2Ph), 4.25−3.10 (m, 11H, (FeC(H)S), NCH_2Ph, $4PCH_2N$), 1.63 (br s, 2H, SCH_2), 1.17 (s, 3H, CH_3), 0.80 (s, 3H, CH_3). ^{31}P{^{1}H} NMR (CD_2Cl_2): δ 23.54 (br s); at −30 °C 26.19 and 22.07 (2d, J = 112 Hz). IR (CH_2Cl_2): ν_{CO} 2094, 2035, and 1965 cm^{-1}. ESI-HRMS (found): m/z 839.0378 (839.0651), $[M - H]^+$; 420.0382 (420.0403), $[M]^{2+}$.

DFT Calculations. The DFT calculations were carried out with Gaussian 09 Version D01 with a functional TPSS and mixed basis sets 6-311+G(d) on Fe and 6-31G(d) on other atoms. The imported crystal structures of **1** and **2** were applied to generate initial geometries of all the species, along with chemically sensible modifications. Geometries from X-ray diffraction analyses of $[\mathbf{1}'(NHN)]^{2+}$ and $[\mathbf{1}']^+$ were also used as references for conformation determinations. There is good agreement between the experimental and calculated metric data, with differences between most bond lengths being less than 1% (Table S5 (Supporting Information)). Additional details of DFT calculations can be found in the Supporting Information.

ASSOCIATED CONTENT

Supporting Information

Text, figures, tables, and CIF, MOL, and MPG files giving preparation and characterization data for all complexes, additional IR, ^{31}P{^{1}H} NMR, and EPR spectra, crystallographic data, and DFT calculation details. This material is available free of charge via the Internet at http://pubs.acs.org.

AUTHOR INFORMATION

Corresponding Authors

symbueno@dlut.edu.cn
mbhall@tamu.edu

Author Contributions

[#]These authors contributed equally to this publication.

Notes

The authors declare no competing financial interest.

■ ACKNOWLEDGMENTS

We are grateful to the Natural Science Foundation of China (Nos. 21373040, 21101057, 21120102036, and 91233201), the Basic Research Program of China (No. 2014CB239402), the Ph.D. Program Foundation of the Ministry of Education of China (No. 20130041110024), the US National Science Foundation (CHE-1266097 to M.Y.D., CHE-1300787 to M.B.H.), the Robert A. Welch Foundation (A-0924 to M.Y.D., A-0648 to M.B.H.), the Swedish Energy Agency, and the K & A Wallenberg Foundation for financial support of this work.

■ REFERENCES

(1) Fan, H.-J.; Hall, M. B. *J. Am. Chem. Soc.* **2001**, *123*, 3828−3829.
(2) Barton, B. E.; Olsen, M. T.; Rauchfuss, T. B. *J. Am. Chem. Soc.* **2008**, *130*, 16834−16835.
(3) Carroll, M. E.; Barton, B. E.; Rauchfuss, T. B.; Carroll, P. J. *J. Am. Chem. Soc.* **2012**, *134*, 18843−188523.
(4) Camara, J. M.; Rauchfuss, T. B. *Nat. Chem.* **2012**, *4*, 26−30.
(5) Capon, J.-F.; Gloaguen, F.; Pétillon, F. Y.; Schollhammer, P.; Talarmin, J. *Coord. Chem. Rev.* **2009**, *253*, 1476−1494.
(6) Tschierlei, S.; Ott, S.; Lomoth, R. *Energy Environ. Sci.* **2011**, *4*, 2340−2352.
(7) Wang, N.; Wang, M.; Chen, L.; Sun, L. *Dalton Trans.* **2013**, *42*, 12059−12071.
(8) Olsen, M. T.; Barton, B. E.; Rauchfuss, T. B. *Inorg. Chem.* **2009**, *48*, 7507−7509.
(9) Camara, J. M.; Rauchfuss, T. B. *J. Am. Chem. Soc.* **2011**, *133*, 8098−8101.
(10) DuBois, M. R.; DuBois, D. L. *Chem. Soc. Rev.* **2009**, *38*, 62−72.
(11) DuBois, D. L.; Bullock, R. M. *Eur. J. Inorg. Chem.* **2011**, 1017−1027.
(12) Helm, M. L.; Stewart, M. P.; Bullock, R. M.; DuBois, M. R.; DuBois, D. L. *Science* **2011**, *333*, 863−866.
(13) Liu, T.; DuBois, D. L.; Bullock, R. M. *Nat. Chem.* **2013**, *5*, 228−233.
(14) Liu, T.; Chen, S.; O'Hagan, M. J.; DuBois, M. R.; Bullock, R. M.; DuBois, D. L. *J. Am. Chem. Soc.* **2012**, *134*, 6257−6272.
(15) Liu, T.; Wang, X.; Hoffmann, C.; DuBois, D. L.; Bullock, R. M. *Angew. Chem., Int. Ed.* **2014**, *53*, 5300−5304.
(16) Wang, N.; Wang, M.; Zhang, T.; Li, P.; Liu, J.; Sun, L. *Chem. Commun.* **2008**, 5800−5802.
(17) Wang, N.; Wang, M.; Liu, J.; Jin, K.; Chen, L.; Sun, L. *Inorg. Chem.* **2009**, *48*, 11551−11558.
(18) Ezzaher, S.; Capon, J.-F.; Gloaguen, F.; Pétillon, F. Y.; Schollhammer, P.; Talarmin, J. *Inorg. Chem.* **2009**, *48*, 2−4.
(19) Lounissi, S.; Zampella, G.; Capon, J.-F.; Gioia, L. D.; Matoussi, F.; Mahfoudhi, S.; Pétillon, F. Y.; Schollhammer, P.; Talarmin, J. *Chem. Eur. J.* **2012**, *18*, 11123−11138.
(20) Wang, Y.; Wang, M.; Sun, L.; Ahlquist, M. S. G. *Chem. Commun.* **2012**, *48*, 4450−4452.
(21) Wang, Y.; Ahlquist, M. S. G. *Dalton Trans.* **2013**, *42*, 7816−7822.
(22) Wang, N.; Wang, M.; Wang, Y.; Zheng, D.; Han, H.; Ahlquist, M. S. G.; Sun, L. *J. Am. Chem. Soc.* **2013**, *135*, 13688−13691.
(23) Bercaw, J. E.; Labinger, J. A. *Proc. Natl. Acad. Sci. U.S.A.* **2007**, *104*, 6899−6900.
(24) Wencel-Delord, J.; Droge, T.; Liu, F.; Glorius, F. *Chem. Soc. Rev.* **2011**, *40*, 4740−4761.
(25) Singleton, M. L.; Bhuvanesh, N.; Reibenspies, J. H.; Darensbourg, M. Y. *Angew. Chem., Int. Ed.* **2008**, *47*, 9492−9495.
(26) Liu, T.; Darensbourg, M. Y. *J. Am. Chem. Soc.* **2007**, *129*, 7008−7009.
(27) Justice, A. K.; Rauchfuss, T. B.; Wilson, S. R. *Angew. Chem., Int. Ed.* **2007**, *46*, 6152−6154.
(28) Justice, A. K.; Gioia, L. D.; Nilges, M. J.; Rauchfuss, T. B.; Wilson, S. R.; Zampella, G. *Inorg. Chem.* **2008**, *47*, 7405−7414.
(29) Hsieh, C.-H.; Erdem, Ö. F.; Harman, S. D.; Singleton, M. L.; Reijerse, E.; Lubitz, W.; Popescu, C. V.; Reibenspies, J. H.; Brothers, S. M.; Hall, M. B.; Darensbourg, M. Y. *J. Am. Chem. Soc.* **2012**, *134*, 13089−13102.
(30) Chouffai, D.; Zampella, G.; Capon, J.-F.; Gioia, L. D.; Gloaguen, F.; Pétillon, F. Y.; Schollhammer, P.; Talarmin, J. *Inorg. Chem.* **2011**, *50*, 12575−12585.
(31) Chouffai, D.; Zampella, G.; Capon, J.-F.; Gioia, L. D.; Goff, A. L.; Pétillon, F. Y.; Schollhammer, P.; Talarmin, J. *Organometallics* **2012**, *31*, 1082−1091.
(32) Yang, J. Y.; Bullock, R. M.; Shaw, W. J.; Twamley, B.; Fraze, K.; Dubois, M. R.; Dubois, D. L. *J. Am. Chem. Soc.* **2009**, *131*, 5935−5945.
(33) Orthaber, A.; Karnahl, M.; Tschierlei, S.; Streich, D.; Stein, M.; Ott, S. *Dalton Trans.* **2014**, *43*, 4537−4549.
(34) Wang, X.; Li, Z.; Zeng, X.; Luo, Q.; Evans, D. J.; Pickett, C. J.; Liu, X. *Chem. Commun.* **2008**, 3555−3557.
(35) Li, B.; Liu, T.; Popescu, C. V.; Bilko, A.; Darensbourg, M. Y. *Inorg. Chem.* **2009**, *48*, 11283−11289.
(36) LeCloux, D. D.; Barrios, A. M.; Mizoguchi, T. J.; Lippard, S. J. *J. Am. Chem. Soc.* **1998**, *120*, 9001−9014.
(37) Herold, S.; Lippard, S. J. *J. Am. Chem. Soc.* **1997**, *119*, 145−156.
(38) Thomas, C. M.; Darensbourg, M. Y.; Hall, M. B. *J. Inorg. Biochem.* **2007**, *101*, 1752−1757.
(39) Munery, S.; Capon, J.-F.; Gioia, L. D.; Elleouet, C.; Greco, C.; Petillon, F. Y.; Schollhammer, P.; Talarmin, J.; Zampella, G. *Chem. Eur. J.* **2013**, *19*, 15458−15461.
(40) Antberg, M.; Dahlenburg, L. *Angew. Chem., Int. Ed. Engl.* **1986**, *25*, 260−261.
(41) Baker, M. V.; Field, L. D. *Aust. J. Chem.* **1999**, *52*, 1005−1012.
(42) Ohki, Y.; Hatanaka, T.; Tatsumi, K. *J. Am. Chem. Soc.* **2008**, *130*, 17174−17186.
(43) Wilson, A. D.; Shoemaker, R. K.; Miedaner, A.; Muckerman, J. T.; DuBois, D. L.; DuBois, M. R. *Proc. Natl. Acad. Sci. U.S.A.* **2007**, *104*, 6951−6956.
(44) O'Hagan, M.; Ho, M.-H.; Yang, J. Y.; Appel, A. M.; DuBois, M. R.; Raugei, S.; Shaw, W. J.; DuBois, D. L.; Bullock, R. M. *J. Am. Chem. Soc.* **2012**, *134*, 19409−19424.